Environmental Science & Technology

Article

pubs.acs.org/est

Indoor Secondary Organic Aerosol Formation Initiated from Reactions between Ozone and Surface-Sorbed D-Limonene

Michael S. Waring*[,†] and Jeffrey A. Siegel[‡,§]

[†]Department of Civil, Architectural and Environmental Engineering, Drexel University, 3141 Chestnut Street, Philadelphia, Pennsylvania 19104, United States

[‡]Department of Civil Engineering, University of Toronto, Toronto, Ontario, Canada

[§]Department of Civil, Architectural and Environmental Engineering, The University of Texas at Austin, Austin, Texas, United States

Supporting Information

ABSTRACT: Reactions between ozone and terpenoids produce numerous products, some of which may form secondary organic aerosol (SOA). This work investigated the contribution to gas-phase SOA formation of ozone reactions with surface-sorbed D-limonene, which is common indoors. A model framework was developed to predict SOA mass formation because of ozone/terpenoid surface reactions, and it was used with steady state experiments in a 283 L chamber to determine the aerosol mass fraction of SOA resulting from surface reactions, ξ_s (the ratio of mass of SOA formed and mass of ozone consumed by ozone/terpenoid surface reactions), for ozone/D-limonene reactions on stainless steel. The ξ_s = 0.70−0.91, with lower relative humidity leading to both higher mass and number formation. Also, surface reactions promoted nucleation more than gas-phase reactions, and number formation due to surface reactions and gas-phase reactions were 126−339 and 51.1−60.2 no./cm^3 per μg/m^3 of formed SOA, respectively. We also used the model framework to predict that indoor spaces in which ozone/D-limonene surface reactions would likely lead to meaningful gas-phase SOA formation are those with surfaces that have low original reactivity with ozone, such as glass, sealed materials, or smooth metals.

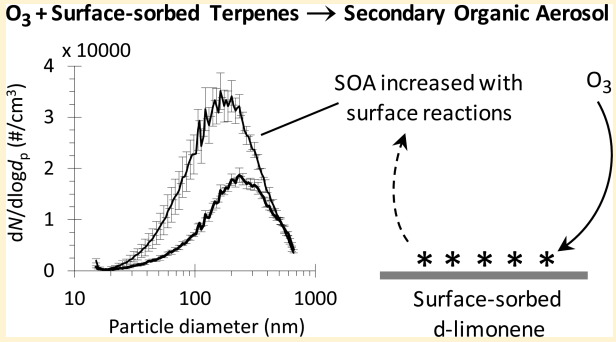

INTRODUCTION

Ozone (O_3) and terpenoids are very common indoors, and their reactions initiate the majority of indoor chemistry. Ozone is often present indoors either due to outdoor-to-indoor transport[1,2] or due to indoor emission from devices, such as ozone or portable ion generators[3−5] or office equipment.[6,7] Terpenoids are directly emitted indoors from off-gassing by wood products[8] and from usage of consumer products such as air fresheners, cleaning agents, and perfumes.[9,10] The most common indoor terpenoids are the monoterpenes ($C_{10}H_{16}$) D-limonene and α-pinene,[11] and their characteristic times of reaction with ozone are often fast enough to compete with the characteristic time of indoor pollutant loss because of air exchange.[12]

Ozone/terpenoid reactions result in myriad compounds, including reactive intermediates, such as hydroxyl radicals, alkylperoxy radicals, and Criegee biradicals; high volatility products, such as carbon dioxide or formaldehyde; and semivolatile products, such as carboxylic acids and hydroperoxides, which may yield secondary organic aerosol (SOA).[13] Indoor SOA formation may be due to nucleation or gas-to-particle partitioning, and indoor formation influences particle distributions in the ultrafine (<0.1 μm) and fine (0.1−2.5 μm) size ranges. Research on indoor-relevant SOA formation has focused almost solely on that which results from products of gas-phase reactions between ozone and pure terpenoids or consumer products.[4,5,14−34] However, rather than focusing on formation because of gas-phase reactions, this paper explores whether the chemistry that occurs due to heterogeneous reactions between ozone and terpenoids sorbed to surfaces may also contribute to the generation of gas-phase SOA indoors.

Surfaces in buildings are complex mixtures of films containing many different reactive organic compounds.[35,36] Terpenoids have vapor pressures that result in moderate sorption to building surfaces from the gas-phase,[37,38] and they are also applied directly to interior surfaces in the form of consumer products.[9,10] The primary loss mechanism of ozone indoors is deposition to interior surfaces,[1,2] so it is conceivable that ozone may react with terpenoids sorbed to surfaces in real buildings. Fick et al. [39] studied ozonolysis of three monoterpenes in an experimental air handling system, and found that the amount of reacted terpenoid (independent of ozone and reaction time) increased with more available surface area. Flemmer et al. [40] challenged with 100 ppb of ozone a surface loaded with sorbed α-terpineol and detected secondary

Received: February 23, 2013
Revised: May 8, 2013
Accepted: May 13, 2013
Published: May 13, 2013

   dx.doi.org/10.1021/es400846d | Environ. Sci. Technol. 2013, 47, 6341−6348

emissions for 72 h. Springs et al.[41] and Shu and Morrison[42] measured the reaction probability, γ (-), which is the ratio of surface reaction rate and collision rate,[43] of ozone and three monoterpenes, Δ^3-carene, D-limonene, and α-terpineol, on beaded surfaces. Surface reaction probabilities ranged from between 2.9×10^{-6} and 3.0×10^{-4}, which are 10−100 times more probable than gas-phase reaction probabilities for the same compounds.

To investigate whether the products of ozone and D-limonene sorbed to surfaces contribute to SOA formation in the gas-phase, we first developed a model framework that describes SOA mass formation because of ozone reactions with a single surface-sorbed terpenoid in terms of an aerosol mass fraction for surface reactions, ξ_s (-), which is defined as the ratio of the mass of SOA formed in the gas-phase and mass of ozone consumed by reactions between ozone and sorbed terpenoids. This framework was used with chamber experiments to quantify ξ_s for reactions between ozone and D-limonene sorbed to stainless steel. We chose D-limonene for our experiments because it readily sorbs to surfaces,[38] is a primary terpenoid in consumer products,[10] is the most common indoor terpenoid,[11,44] reacts with ozone on surfaces,[39,41] and has high mass formation potential.[45] The results from the experiments are then extrapolated to common indoor surfaces to explore the role of SOA formation because of ozone reactions with surface-sorbed organic compounds in typical indoor environments.

METHODOLOGY

Model Framework. To predict SOA generated by ozone/terpenoid surface reactions, the model must isolate the fraction of ozone that reacts with the sorbed terpenoid on the surface, as opposed to ozone that reacts with another surface moiety. Irreversible loss to surfaces indoors is quantified with the deposition velocity, v_d (m/h), which is a mass transfer coefficient defined as the ratio of the bulk concentration to the flux to the surface. First, we use the model of Cano−Ruiz et al.[43] to describe the ozone deposition velocity to an "original surface" (i.e., without terpenoid sorption), $v_{d,o}$ (m/h), as in eq 1:

$$v_{d,o} = \left(\frac{1}{v_t} + \frac{4}{\gamma_o \langle v \rangle} \right)^{-1} \quad (1)$$

where v_t (m/h) is the transport limited deposition velocity, γ_o is the reaction probability of the original surface, and $\langle v \rangle$ is the Boltzmann velocity (1.296×10^6 m/h for O_3 at 296 K). Equation 1 represents the deposition velocity as the inverse sum of two resistances in series: the mass transport resistance through the boundary layer and the reaction rate resistance at the material surface. The reactivity of the surface dictates the influence of each resistance; as $\gamma_o \to 1$, the mass transport is rate limiting and $v_{d,o} \approx v_t$, and as $\gamma_o \to 0$, the reactions are rate limiting and $v_{d,o} \approx \gamma_o \langle v \rangle / 4$. One can approximate $v_t \approx u^*/\Gamma$, where u^* (m/h) is the friction velocity and Γ is a nondimensional factor that results from integrating the ratio of kinematic viscosity to the ozone diffusivity throughout the boundary layer.[46]

For a surface with sorbed reactants, eq 1 must be modified to represent irreversible loss with a three-resistor model: one boundary layer mass transport resistance in series with two parallel resistances representing ozone reaction with the original surface, as well as the sorbed compound.[41,47] The modified expression for the deposition velocity to the loaded surface, $v_{d(o+terp)}$ (m/h), is

$$v_{d,(o+terp)} = \left(\frac{1}{v_t} + \frac{4}{\gamma_{(o+terp)} \langle v \rangle} \right)^{-1} \quad (2)$$

where $\gamma_{(o+terp)}$ is the overall reaction probability of the surface, defined as the fractional sum of the reaction probability for sites without and with sorbed terpenoids

$$\gamma_{(o+terp)} = (1 - r_{terp})\gamma_o + r_{terp}\gamma_{terp} \quad (3)$$

where γ_{terp} is the reaction probability of the sorbed terpenoid and r_{terp} is the fractional coverage of a surface with the sorbed terpenoid. The fraction of ozone that reacts on the surface with only sorbed terpenoids is defined as $f_{O_3/terp}$, which for more than monolayer coverage is 1 and for less than monolayer coverage is[47]

$$f_{O_3/terp} = \frac{r_{terp}\gamma_{terp}}{\gamma_{(o+terp)}} \quad (4)$$

Finally, the deposition velocity of ozone solely to the sorbed terpenoids, $v_{d,terp}$ (m/h), may be calculated with the product of the fraction of ozone reacting with the terpenoid and the overall deposition velocity to the loaded surface:

$$v_{d,terp} = f_{O_3/terp} v_{d,(o+terp)} \quad (5)$$

Once ozone reacts with surface-sorbed terpenoids, the various products partition among the particle, gas, and surface phases,[36] and that fraction partitioning to the particle phase yields SOA mass. Some of these products may further react with ozone or the hydroxyl radical, which is formed from ozone/terpenoid reactions,[12] and these secondary products may also partition to SOA or other available surfaces. Taking all of these possibilities into account, we define an "effective aerosol mass fraction of gas-phase SOA formed due to products initiated by ozone/terpenoid surface reactions" as ξ_s, which is the ratio of the mass of SOA formed to the mass of ozone consumed solely by the ozone and terpenoid surface reactions. Using ξ_s, the contribution of ozone/terpenoid surface reactions on a single material to gas-phase SOA may be incorporated into a volume-normalized mass balance on C_{SOA} ($\mu g/m^3$), the concentration of SOA in the gas-phase.[48] Assuming isothermal conditions, no particle resuspension, and well-mixed air with only one terpenoid, C_{SOA} is predicted with eq 6:

$$\frac{dC_{SOA}}{dt} = \lambda C_{SOA,inlet} + \xi_g k C_{O_3,m} C_{terp,m} G + \xi_s C_{O_3} v_{d,terp} \frac{A}{V} - (\lambda + \beta_{SOA}) C_{SOA} \quad (6)$$

where λ (h^{-1}) is the air exchange rate; $C_{SOA,inlet}$ ($\mu g/m^3$) is the concentration of SOA entering with the inlet air; ξ_g (-) is the aerosol mass fraction for SOA formed because of ozone/terpenoid gas-phase reactions, which is the ratio of the mass of SOA formed and mass of terpenoid consumed by gas-phase reactions;[49] k (ppb^{-1} h^{-1}) is the ozone/terpenoid gas-phase reaction rate constant; $C_{O3,m}$ and $C_{terp,m}$ (ppb) and are the mole fractions of the ozone and terpenoid, respectively; C_{O3} ($\mu g/m^3$) is the mass concentration of ozone; G is a conversion factor to change units from ppb to $\mu g/m^3$ for the terpenoid mole fraction; A (m^2) is the surface area; V (m^3) is the gas volume; and β_{SOA} (h^{-1}) is the surface loss rate of SOA. In eq 6, the term

on the left-side is the time rate of change of C_{SOA} in the gas-phase. The first three terms on the right-side are SOA source mechanisms, which are introduction with air exchange, formation due to gas-phase reactions, and formation due to surface reactions, respectively. The last two terms are SOA loss mechanisms, which are removal by air exchange and deposition, respectively.

Chamber Experiments. To isolate the effect of surface reactions on gas-phase SOA formation, we used laboratory chamber experiments in a V = 283 L stainless-steel reaction chamber system, which is shown schematically in Figure S1 in the Supporting Information (SI). The chamber system was operated as a continuously mixed flow reactor (CMFR). The experiments were run with constant conditions for at least 12 h until steady state was reached, and measured values are for the last hour of the experiments. Our objective was to measure SOA formation while holding the chamber air exchange rate, ozone, and D-limonene mole fractions nearly constant, but while varying the area-to-volume ratio (A/V in eq 6) across experiments. This approach elucidates differences in SOA formation that are due to surface reactions. We operated experiments at two different A/V configurations: Chamber 1 was the empty stainless-steel chamber, and Chamber 2 was the chamber plus 14 stainless-steel woven wire screens. The addition of the stainless-steel screens increased the A by 460% and decreased V by 2%, which changed the total A/V from Chamber 1 to Chamber 2 by 469%.

There were two inlet airflow paths into the chamber, the primary and D-limonene flows, and one outlet flow. For the primary inlet flow, desired values of relative humidity (RH) and ozone were achieved by adjusting bypass valves, and the volumetric flow of air was controlled with a mass flow controller (Aarlborg GFC37) at 3.6 L/min (Sensidyne Gilian Gilibrator-2). The RH and temperature (TSI Q-Trak 8551) and ozone mole fraction (2B Technologies 202) were measured at the chamber inlet every five minutes. The D-limonene inlet flow was controlled (Aarlborg GFC171S) to regulate a flow of nitrogen at 5 mL/min through a diffuser with liquid D-limonene (Sigma-Aldrich, 98% purity). Outlet ozone was sampled with the same ozone monitor as the primary inlet. Particle size distributions were sampled at the outlet with a scanning mobility particle sizer (SMPS) over 106 bins in the range of 15.1−661 nm (TSI 3936L85) every 5 min. The D-limonene was sampled at the outlet onto Tenax GR-packed focus liners (Atas A100094) for 4 min at a flow rate of 44 mL/min (Buck VSS-1) for a total sample volume of 0.176 L. The D-limonene was analyzed by thermal desorption, gas chromatography, flame ionization detection, TD/GC-FID (Agilent G1530A; Atas Optic 2 thermal desorber), with the method in the SI. Breakthrough was less than 2% for the highest mole fraction at this flow rate. Artifacts in photometric ozone measurements may exist at high terpenoid mole fractions, so we quantified that interference with only D-limonene at certain mole fractions with no ozone, and then subtracted off that interference from the ozone readings during the SOA formation experiments. For ozone parameters, the uncertainty is the quadrature sum of the instrument accuracy (>of 1.5 ppb or 2% of reading) and the standard deviation during the steady state period. The D-limonene uncertainty is two standard deviations of daily calibration standards.

Application of Model Framework to Experiments. The model framework was applied to 12 steady state chamber experiments (SOA1−SOA12) to calculate ξ_s because of ozone reactions with sorbed D-limonene. Discrete sets of experiments at RH = 20%, 50%, and 70% were conducted with similar chamber flows and reactant mole fractions but with either Chamber 1 or Chamber 2 area conditions. In all experiments, inlet particle concentrations were negligibly small, so eq 6 can be solved for C_{SOA} at steady state as shown in eq 7:

$$C_{SOA} = \frac{\xi_g k C_{O_3,m} C_{terp,m} G + \xi_s C_{O_3} \nu_{d,terp} \frac{A}{V}}{\lambda + \beta_{SOA}} \quad (7)$$

Since D-limonene was used, in any equations the subscript "terp" refers to D-limonene. Then, we defined $C_{SOA,1}$ ($\mu g/m^3$) and $C_{SOA,2}$ ($\mu g/m^3$) as the SOA mass concentrations for the Chamber 1 and Chamber 2 conditions, respectively. After expanding eq 7 to include deposition to the walls in Chamber 1 and the walls or the screens in Chamber 2, we subtracted $C_{SOA,1}$ from $C_{SOA,2}$ and solved for ξ_s:

$$\xi_s = [L_1 L_2 (C_{SOA,2} - C_{SOA,1}) - kG(L_1 \xi_{g,2} C_{O_3,m,2} C_{terp,m,2} - L_2 \xi_{g,1} C_{O_3,m,1} C_{terp,m,1})]/[L_1 C_{O_3,2} \left(\left(\nu_{d,terp} \frac{A}{V} \right)_{2w} + \left(\nu_{d,terp} \frac{A}{V} \right)_{2s} \right) - L_2 C_{O_3,1} \left(\nu_{d,terp} \frac{A}{V} \right)_{1w}] \quad (8)$$

where any subscript "1" or "2" refers to Chamber 1 or Chamber 2, respectively, "1w" are the wall surfaces in Chamber 1, "2w" are the walls in Chamber 2, and "2s" are the stainless-steel screens in Chamber 2 and L is the total SOA loss rate, which is $(\lambda + \beta_{SOA})$ (h^{-1}). To determine the C_{SOA} for eq 8, the SOA size distributions measured by the SMPS were converted to mass concentrations by assuming spherical particles with a density of 1 g/cm^3. Thus, we actually report a "normalized" ξ_s, which one can adjust by multiplying by a density of choice.

Parameters used in eq 8 were as follows: For the flow rate of 3.6 L/min, the air exchange rate for Chamber 1 was λ_1 = 0.76 h^{-1} and for Chamber 2 was λ_2 = 0.78 h^{-1}. The SOA deposition was estimated [50] for Chamber 1 as $\beta_{SOA,1}$ = 0.030 h^{-1} and for Chamber 2 as $\beta_{SOA,2}$ = 0.14 h^{-1}. Since $L = (\lambda + \beta_{SOA})$, L_1 = 0.79 h^{-1} and L_2 = 0.92 h^{-1}. The area-to-volume ratios were $(A/V)_{1w}$ = 9.19 m^{-1}, $(A/V)_{2w}$ = 9.37 m^{-1}, and $(A/V)_{2s}$ = 33.7 m^{-1}. The k = 0.018 ppb^{-1} h^{-1}, [51] and ξ_g was estimated as describe in the SI. All other parameters in eq 8 were measured directly, with the exception of the $\nu_{d,terp}$ for different surfaces i, which was calculated by combining eqs 1−5 and assuming that the ozone deposition occurring is in the reaction rate limiting regime (which is later verified), so that

$$\nu_{d,terp,i} = \left(\frac{\gamma_{terp}}{\gamma_{terp} - \nu_{d,o,i} \frac{4}{\langle v \rangle}} \right) (\nu_{d,(o+terp),i} - \nu_{d,o,i}) \quad (9)$$

Note that eq 9 is defined so long as $\gamma_{terp} \neq \gamma_{o,i}$, which is true for the surfaces used in this work. To use eq 9 in eq 8, γ_{terp} for D-limonene was assumed as 10^{-4}, [4,41] and steady state mass balances were used to determine $\nu_{d,(o+terp)}$ and $\nu_{d,o}$ for all surfaces combined in Chamber 1 and Chamber 2. To calculate $\nu_{d,(o+terp)}$, ozone measurements from the SOA formation experiments (SOA1−SOA12) were used. Also, $\nu_{d,o}$ was determined for the original surfaces without D-limonene with an initial set of 12 experiments (O1−O12) occurring prior to any SOA formation experiments. These original deposition velocities followed a power-law fit as a function of the ozone

dx.doi.org/10.1021/es400846d | Environ. Sci. Technol. 2013, 47, 6341−6348

Table 1. Steady State Inlet and Mean (And Standard Deviation/Uncertainty) Chamber Concentrations for SOA Formation Experiments, SOA1−SOA12, Occurring in Chambers with Different Surface Areas and Relative Humidity (RH)

			inlet	well-mixed chamber outlet					
			ozone	ozone	D-limonene[c]	SOA mass	SOA number[d]		
exp.[a]	chamber area[b]	RH (%)	$C_{O3,m,inlet}$ (ppb)	$C_{O3,m}$ (ppb)	$C_{terp,m}$ (ppb)	C_{SOA} ($\mu g/m^3$)	$C_{SOA,N}$ (no./cm^3)	GM (nm)	GSD
SOA1	Ch1	20	127	5.7 (1.5)	630 (32)	218 (2.7)	12 600 (300)	238	1.95
SOA2	Ch2	20	221	5.3 (1.8)	483 (24)	266 (7.0)	24 700 (2100)	178	2.05
SOA3	Ch2	20	217	6.9 (1.6)		250 (3.7)	25 600 (1500)	166	1.99
SOA4	Ch2	20	215	7.1 (1.7)	417 (21)	248 (5.1)	24 500 (1200)	169	2.01
SOA5	Ch1	50	120	5.3 (1.6)	632 (32)	193 (3.1)	11 900 (100)	225	2.00
SOA6	Ch1	50	127	5.1 (1.7)	671 (34)	219 (2.6)	12 900 (100)	231	2.00
SOA7	Ch2	50	227	4.4 (1.5)	469 (23)	227 (6.9)	17 700 (1100)	201	1.92
SOA8	Ch2	50	226	6.5 (1.6)	388 (19)	262 (5.5)	20 900 (400)	197	1.94
SOA9	Ch1	70	124	4.2 (1.6)	660 (33)	187 (5.7)	9 580 (200)	250	2.00
SOA10	Ch2	70	251	4.8 (1.8)	400 (20)	250 (4.2)	17 400 (800)	212	1.98
SOA11	Ch1	50	223	14 (1.6)	634 (32)	299 (7.8)	14 400 (500)	262	1.93
SOA12	Ch1	50	409	29 (1.5)	413 (21)	359 (9.8)	15 700 (500)	280	1.90

[a]Experiment number. [b]SOA formation was assessed in a chamber with two different surface area to volume ratios (A/V): Chamber 1 (Ch1) was the empty stainless steel chamber with an A/V = 9.19 m^{-1}, and Chamber 2 (Ch2) was the same chamber plus 14 stainless steel screens with an A/V = 43.1 m^{-1}. [c]The D-limonene mole fraction for SOA3 was not reported or included in calculations due to an instrument error during that experiment. [d]Unimodal log-normal size distributions were fit to the steady state particle size distributions, GM = geometric mean diameter (nm) and GSD = geometric standard deviation.

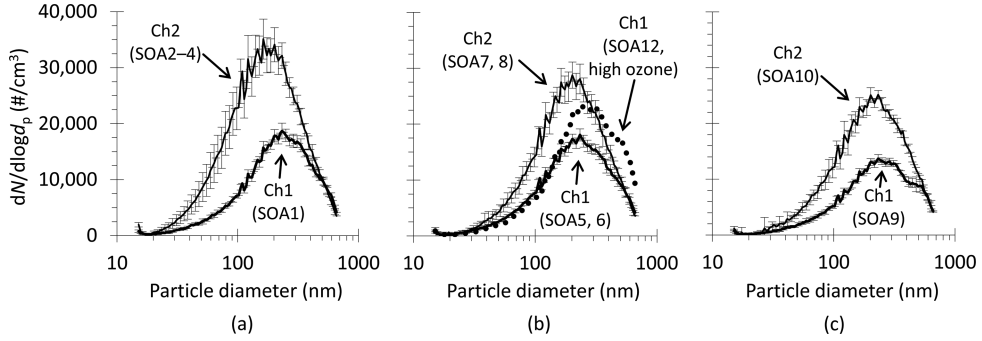

Figure 1. Differences in mean steady state SOA size distributions (standard deviation shown by whiskers) for Chamber 1 (Ch1, surface area to volume ratio of 9.2 m^{-1}) and Chamber 2 (Ch2, surface area to volume ratio of 43 m^{-1}) experiments at (a) RH = 20%, (b) RH = 50%, and (c) RH = 70%. The experiments comprising each distribution are in parentheses; experiment SOA12 is also shown, which was conducted at higher ozone mole fractions at RH = 50%.

chamber mole fraction, and these fits were used in the SOA formation experiments to estimate the $v_{d,o}$ with D-limonene present in the chamber. These total chamber deposition velocities were then used to determine the deposition velocities to the individual chamber surfaces (i.e., 1w, 2w, or 2s) with area-to-volume ratio weighted averages. Results from experiments O1−O12 and details on these deposition velocity calculations are in the SI.

RESULTS AND DISCUSSION

SOA Formation. Table 1 lists the steady state results from the SOA formation experiments SOA1−SOA12, grouped by chamber area and RH conditions, for $C_{O3,m}$, C_{SOA}, and $C_{SOA,N}$ (no./cm^3), which is the SOA number concentration. The results demonstrate that more SOA number and mass were formed in Chamber 2 experiments with the higher surface area, for all RH conditions. The SOA formation in Chamber 2 over Chamber 1 was relatively larger from a number than mass perspective. For instance, for the average results at RH = 50%, the C_{SOA} increased by 19% while the $C_{SOA,N}$ increased by 56%. So that $C_{O3,m}$ in Chamber 2 would be near the magnitude of $C_{O3,m}$ in Chamber 1, the inlet ozone mole fraction, $C_{O3,m,inlet}$ (ppb), was greater for the Chamber 2 than the Chamber 1 experiments because of the larger A/V in Chamber 2. The D-limonene mole fraction is lower in the Chamber 2 experiments since its emission into the chamber was not varied and more D-limonene was consumed by surface reactions in Chamber 2. Thus, larger SOA formation occurred in Chamber 2 over Chamber 1 even though the product of ozone and D-limonene mole fractions, which is a governing factor for SOA formation due to gas-phase reactions, was always lower in Chamber 2 than Chamber 1 experiments.

Figure 1 displays the means (and standard deviations) of the steady state SOA size distributions for experiments in Chamber 1 and Chamber 2 with identical RH. Table 1 also lists a unimodal log-normal fit to those distributions. This fit could be improved with additional modes, but a unimodal fit was used for clarity in trends. For all RH, the geometric mean (GM) diameter for the mean distribution for Chamber 2 shifted to the smaller particle sizes with respect to Chamber 1, since the enhanced particle number concentration in Chamber 2 provided more sorptive reservoirs to which SOA-forming products could partition. More absolute SOA number formation occurred at the lower RH conditions, potentially

dx.doi.org/10.1021/es400846d | Environ. Sci. Technol. 2013, 47, 6341−6348

because extra water vapor inhibits formation of stabilized Criegee intermediates, which are correlated with nucleation potential.[52] The geometric standard deviations (GSD) were similar for Chamber 1 and Chamber 2, indicating similarity in the distribution widths. These mean distributions for Chamber 1 and Chamber 2, regardless of RH, divided from one into two distinct distributions near a particle diameter of 20 nm and converged at diameters greater than about 500 nm. Therefore, it appears that at our experimental conditions the differences that occur for SOA number and mass formation are for SOA with diameters less than ∼500 nm.

To further demonstrate that the SOA formation differences in Chamber 1 and Chamber 2 were due to surface reaction effects as opposed to higher gas-phase mole fractions, experiments SOA11 and SOA12 were performed with Chamber 1 at RH = 50% but with increased ozone mole fractions. Both SOA11 and SOA12 exhibited higher mass and number formation than the Chamber 1 experiments of SOA5 and SOA6. However, SOA11 and SOA12 exhibited higher mass formation but lower number formation than the Chamber 2 experiments of SOA7 and SOA8. To further illustrate this distinction, the steady state distribution from experiment SOA12 is also plotted in Figure 1b. For SOA12, the size distribution diverged from that of experiments SOA5 and SOA6 in Chamber 1 at a diameter of ∼105 nm and never rejoined the distribution at higher diameters, as did experiments SOA7 and SOA8 in Chamber 2. Also, the GM diameters for SOA11 and SOA12 shifted to the right of those of SOA5 and SOA6 in Chamber 1, rather than the left, as with the size distributions in the SOA7 and SOA8 experiments in Chamber 2. Thus, the enhanced SOA formed from increased surface reactions in Chamber 2 has a pattern distinct from that formed from higher gas-phase reactant mole fractions, with surface reactions leading to lower mass formation and higher number formation with smaller diameter particles.

SOA Formation Initiated by Surface Reactions. Results from the SOA formation experiments in Chamber 1 and Chamber 2 were used to determine the effective aerosol mass fraction for SOA due to ozone and D-limonene surface reactions, excluding SOA11 and SOA12. At RH = 20%, 50%, and 70%, the ξ_s = 0.91 (0.87), 0.84 (0.70), and 0.70 (0.65), respectively, where parenthetical values represent the uncertainty propagated through the relevant calculations. Higher formation may be associated with lower RH values, but this trend is within the result uncertainty, which is admittedly high and mostly due to the relatively high ozone uncertainty at low chamber ozone mole fractions. Aerosol number fractions were not calculated similar to mass fractions because number formation due to gas-phase reactions is much less understood than mass formation. However, to explore the differences between the gas-phase versus surface reactions on number formation, we also estimated the ratio of the number of particles formed per mass of SOA formed from both the surface-phase, X_s, and gas-phase, X_g, reactions. We found that X_s = 339, 179, and 126 no./cm^3 per μg/m^3 and X_g = 57.7, 60.2, and 51.1 no./cm^3 per μg/m^3, for RH = 20%, 50%, and 70%, respectively. Comparing X_s and X_g illustrates the different nucleation potentials between the two reaction types at different RH. The X_s was higher at the lower RH values, again consistent with evidence that larger number formation occurs for ozone/D-limonene reactions at lower RH.

The SOA surface mass fractions are a factor of ∼1.1−1.5 higher than gas-phase aerosol mass fractions over all experiments, which were ξ_g = 0.59−0.62. However, ξ_s and ξ_g are defined with different denominators (the mass of ozone consumed for ξ_s and mass of D-limonene consumed for ξ_g), so we also estimated $\xi_{s,terp}$, which is the surface aerosol mass fraction defined as the ratio of the mass of SOA formed to that of D-limonene consumed by surface reactions, assuming a one-to-one molar reaction. The $\xi_{s,terp}$ = 0.25−0.32, which is a factor of 0.38−0.54 lower than ξ_g. One would expect $\xi_{s,terp}$ to be lower than ξ_g because the semivolatile products resulting from surface reactions must partition from the surface → air → particle phase to form SOA mass rather than only from the air → particle phase (as for SOA from gas-phase reactions), and some of these products likely remain bound to the surface.[36] Similar to ξ_g, the term ξ_s (and also $\xi_{s,terp}$) should be a function of the amount of organic material present in the air,[49] and so it is likely not constant but will decrease when SOA concentrations are less than those in our experiments and vice versa.

Deposition Velocities and Surface Reactivity. For eq 9 to be valid for use in eq 8 to calculate the surface aerosol mass fraction, the deposition velocities must be in the reaction rate limited regime. The $v_{d,o}$ were 0.20−0.23 m/h for the chamber walls and 0.10−0.12 m/h for the screens, and $v_{d,(o+terp)}$ were 0.53−1.1 m/h for the walls and 0.37−0.66 m/h for the screens, generally lower than for most surfaces indoors.[53] Using these experimental data and the theory of Morrison and Nazaroff,[46] we estimated u^* = 3 cm/s and the transport limited deposition velocity as v_t = 8.1 m/h, and we have plotted the deposition velocities as a function of the surface reaction probability in Figure S3 in the SI. All values are in the reaction rate limited regime, confirming the appropriateness of eq 9 in this work, and $v_{d,terp}$ = 0.61−0.82 m/h for the different surfaces. Higher RH led to higher $v_{d,terp}$, potentially due to ozone reactions with water, so surface mass fractions at higher RH may be somewhat artificially reduced. Using eqs 1 and 2, we calculated for both Chamber 1 and Chamber 2 that $\gamma_o = (3.1-7.1) \times 10^{-7}$ and $\gamma_{(o+terp)} = (1.2-3.4) \times 10^{-6}$, signifying both that the D-limonene sorption increased the surface reactivity by an order of magnitude and that there was less than monolayer coverage by the D-limonene in all experiments. Values of $f_{O3/terp}$ = 0.27−0.88 and r_{terp} = 0.0084−0.027 over all experiments, and these r_{terp} are very near those fractional coverages for comparable surfaces and D-limonene mole fractions.[11] Surface-specific values for these parameters are in the SI.

Application to Real Indoor Environments. For typical indoor conditions, we explored the ranges of magnitudes of ozone reactions with sorbed D-limonene on various surfaces and the SOA formed from those reactions, using the model and our experimental results. Indoor surfaces have reaction probabilities of $\gamma_o = 10^{-8}$ to 10^{-4}. For instance, $\gamma_o \leq 10^{-6}$ is common for glass, metals, and sealed ceramics, $\gamma_o \approx 10^{-5}$ for aged carpet, and $\gamma_o \approx 10^{-4}$ for new carpet and brick.[43,54] Figure 2a−c plots the ozone deposition velocity to D-limonene as a function of fractional coverage for surfaces with $\gamma_o = \{10^{-8}, 10^{-7}, 10^{-6}, 10^{-5}, 10^{-4}\}$ for different friction velocities of $u^* = \{0.3, 1, 3$ cm/s$\}$, using eqs 2−5 and assuming $\gamma_{terp} = 10^{-4}$ and RH = 50%. The r_{terp} values were used to estimate a gas-phase D-limonene mole fraction based on a linear relationship from our experiments, and these $C_{terp,m}$ are shown in parentheses and are 3.5−3500 ppb. Indoor mole fractions of D-limonene are capable of reaching ∼1,000 ppb because of consumer product use,[10,22] but time-averaged mole fractions of less than ∼100 ppb are common;[44] therefore, r_{terp} may be less than ∼0.01 indoors and $v_{d,terp}$ should reside in the reaction rate limited regime in most

dx.doi.org/10.1021/es400846d | Environ. Sci. Technol. 2013, 47, 6341−6348

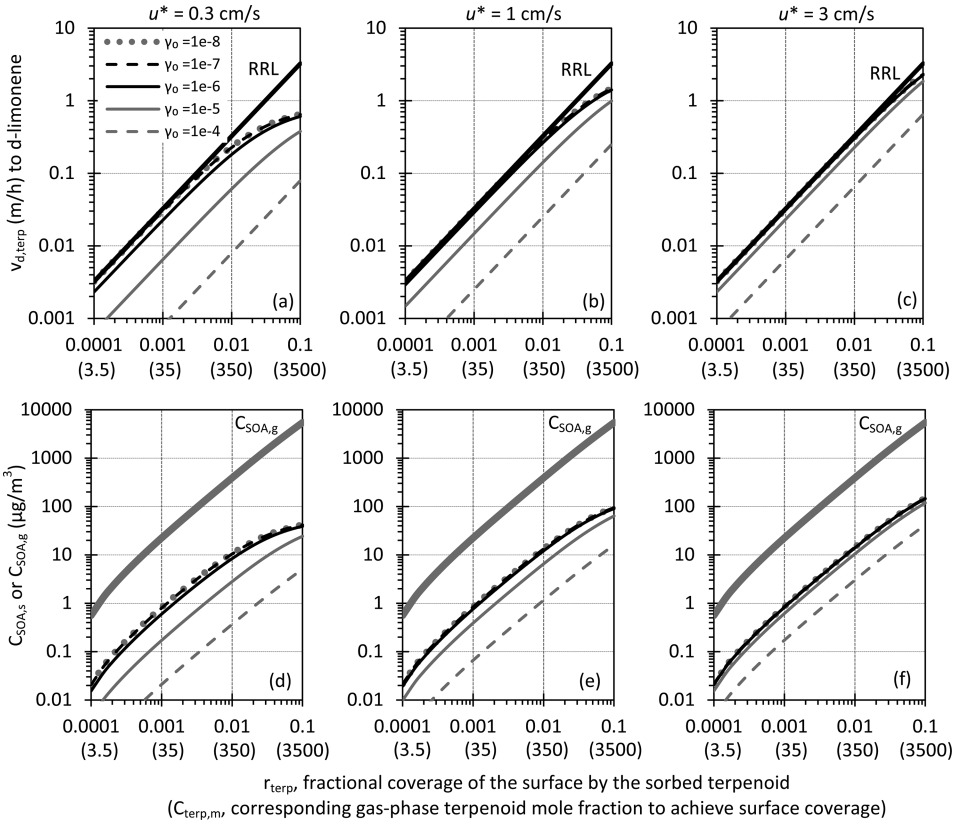

Figure 2. Ozone deposition velocity to D-limonene ($v_{d,terp}$) as a function of fractional coverage (r_{terp}), for five different surfaces with γ_o that represent the range of common indoor materials at friction velocities of u^* = (a) 0.3, (b) 1, and (c) 3 cm/s, estimated using eqs 2−5 and assuming $\gamma_{terp} = 10^{-4}$. The thick black line plots a−c are the deposition velocities if one combines eqs 2, 4, and 5 and assumes $v_{d,(o+terp)}$ is reaction rate limited (RRL). Plots d−f display the SOA formed because of surface ($C_{SOA,s}$) and gas-phase ($C_{SOA,g}$) reactions for those same conditions assuming ozone is at 10 ppb. The thick gray line on each of plots d−f is the $C_{SOA,g}$, and all other lines are the $C_{SOA,s}$ for the different γ_o. See text for details.

spaces. For cases with higher r_{terp}, the $v_{d,terp}$ converge to the same value independent of γ_o because the D-limonene approaches monolayer coverage on the surface, making reaction sites essentially identical and $v_{d,terp} \approx v_t$ (not shown in Figure 2 as it occurs between r_{terp} = 0.1−1).

The range of u^* explored is characteristic of indoors,[46,50] and increasing u^* increases the $v_{d,terp}$ for the same r_{terp} since v_t also increases, which lowers the transport resistance of the ozone through the boundary layer. On Figure 2a−c, the dark line is $v_{d,terp}$ if one combines eqs 2, 4, and 5 and assumes $v_{d,(o+terp)}$ is reaction rate limited (RRL), which is represented by eq 10:

$$v_{d,terp,RRL} = \frac{r_{terp}\gamma_{terp}\langle v\rangle}{4} \quad (10)$$

For materials with $\gamma_o \leq 10^{-6}$, the $v_{d,terp,RRL}$ estimated with eq 10 is near the actual $v_{d,terp}$ predicted by eqs 1−5, especially for lower values of r_{terp} and higher values of u^*. Thus, for surfaces for which ozone reactivity is low (i.e., when $\gamma_o \leq \sim 10^{-6}$) or when the airflow indoors is turbulent, the $v_{d,terp}$ tends to depend only on r_{terp}, assuming γ_{terp} is the same for different surfaces. Figure 2a−c also illustrate that at lower r_{terp}, the γ_o has a large impact on the $v_{d,terp}$ for that material, and there are three distinct depositional regimes for materials with $\gamma_o = 10^{-6}$ or less, 10^{-5}, or 10^{-4}. The distinctiveness of these regimes depends on u^*, since at lower u^*, the transport resistance of $v_{d,terp}$ is higher, which decreases the $v_{d,terp}$ more than for higher u^* at comparable γ_o. Since the SOA formed from surface reactions scales with $v_{d,terp}$, the magnitude of SOA formed by ozone/D-limonene surface reactions will be larger because of reactions on surfaces with low γ_o than on surfaces with high γ_o at the same r_{terp} and u^*.

Reaction probabilities were discussed thus far in context of particular surfaces, but the model is also applicable to an average γ_o for an indoor space when predicting SOA formation. As such, we modeled the contributions to C_{SOA} from surface reactions and gas-phase reactions at steady state with eq 7 assuming $C_{O_3,m}$ = 10 ppb, λ = 0.5 h^{-1}, β_{SOA} = 0.1 h^{-1}, and A/V = 3 m^{-1}. The $v_{d,terp}$ are identical to those shown in Figure 2a−c at corresponding values of γ_o and r_{terp} (and therefore $C_{terp,m}$). The aerosol mass fractions due to gas-phase reactions were determined according to the method in the SI, and the surface aerosol mass fraction was estimated according to our experimental observations as $\xi_s = 1.38 \cdot \xi_g$. Results are in Figure 2d−f. The three depositional regimes observed for $v_{d,terp}$ translate into the same three regimes of SOA formation due to surface reactions. Some modeled conditions are not typical and are extreme cases, for example, $C_{terp,m}$ > 1000 ppb or $\gamma_o = 10^{-8}$. Two representative indoor conditions are that of u^* = 1 cm/s and r_{terp} = 0.001 (i.e., $C_{terp,m}$ = 35 ppb) with a γ_o of either 10^{-5} or 10^{-6}. At these two conditions, $C_{SOA,g}$ = 22 $\mu g/m^3$ and $C_{SOA,s}$ = 0.39 and 0.76 $\mu g/m^3$, respectively, so that of the total SOA formed ∼1.7% and 3.4%, respectively, of the mass is due to the surface reaction impacts. If the number formation trends observed in our experiments are used as an estimate, ∼5.1% and 10%, respectively, of SOA number would be the result of surface reactions. For indoor spaces with lower γ_o or higher u^*,

dx.doi.org/10.1021/es400846d | Environ. Sci. Technol. 2013, 47, 6341−6348

these fractions of SOA because of surface reactions would tend to increase.

Therefore, SOA formation due to surface reactions is likely to occur on originally nonreactive surfaces, such as glass or smooth metals. However, real indoor surfaces may be coated with organic films,[35,36] which could increase original reaction probabilities on these materials and reduce formation. Moreover, the relationship between the gas-phase and surface reaction aerosol mass fractions needs more investigation since it may not hold at different SOA or reactant concentrations. The impact of humidity on $v_{d,terp}$ needs refinement as well, as we only measured limited results at conditions other than RH = 50%. Also, other terpenoids would exhibit differences in formation. For instance, Δ^3-carene has sorptive characteristics that are similar to D-limonene but it has lower gas-phase SOA mass fractions and a lower γ_{terp},[41] so it would have less formation; also, α-terpineol is more sorptive than D-limonene,[42] but it likely has lower mass fractions, so the impact on formation is uncertain. In sum, our results provide evidence that SOA may be formed because of ozone reactions with D-limonene sorbed onto surfaces, though their application to surfaces in indoor environments require additional field experiments to verify the extent and importance of such reactions.

■ ASSOCIATED CONTENT

Supporting Information

(1) Schematic of the small chamber system, (2) method for measuring D-limonene with GC/FID, (3) method to determine the aerosol mass fraction for SOA formed due to gas-phase reactions, (4) deposition velocity calculation procedure, and (5) surface parameter results. This information is available free of charge via the Internet at http://pubs.acs.org/.

■ AUTHOR INFORMATION

Corresponding Author

*E-mail: msw59@drexel.edu.

Notes

The authors declare no competing financial interest.

■ ACKNOWLEDGMENTS

This work was funded by the National Science Foundation (Awards 1055584 & DGE 0549428) and the Harrington Dissertation Fellowship from the University of Texas at Austin.

■ REFERENCES

(1) Sabersky, R. H.; Sinema, D. A.; Shair, F. H. Concentrations, decay rates, and removal of ozone and their relation to establishing clean indoor air. *Environ. Sci. Technol.* **1973**, 7 (4), 347−353, DOI: 10.1021/es60076a001.

(2) Weschler, C. J. Ozone in indoor environments: Concentration and chemistry. *Indoor Air* **2000**, *10*, 269−288, DOI: 10.1034/j.1600-0668.2000.010004269.x.

(3) Britigan, N.; Alshawa, A.; Nizkorodov, S. A. Quantification of ozone levels in indoor environments generated by ionization and ozonolysis air purifiers. *J. Air Waste Manage.* **2006**, *56*, 601−610, DOI: 10.1080/10473289.2006.10464467.

(4) Waring, M. S.; Siegel, J. A.; Corsi, R. L. Ultrafine particle removal and generation by portable air cleaners. *Atmos. Environ.* **2008**, *42* (20), 5003−5014, DOI: 10.1016/j.atmosenv.2008.02.011.

(5) Waring, M. S.; Siegel, J. A. The effect of an ion generator on indoor air quality in a residential room. *Indoor Air* **2011**, *21* (4), 267−76, DOI: 10.1111/j.1600-0668.2010.00696.x.

(6) Lee, S. C.; Lam, S.; Fai, H. K. Characterization of VOCs, ozone, and PM10 emissions from office equipment in an environmental chamber. *Build. Environ.* **2001**, *36*, 837−842, DOI: 10.1016/S0360-1323(01)00009-9.

(7) Destaillats, H.; Maddalena, R. L.; Singer, B. C.; Hodgson, A. T.; McKone, T. E. Indoor pollutants emitted by office equipment: A review of reported data and information needs. *Atmos. Environ.* **2008**, *42* (7), 1371−1388, DOI: 10.1016/j.atmosenv.2007.10.080.

(8) Baumann, M. G. D.; Batterman, S. A.; Zhang, G.-Z. Terpene emissions from particleboard and medium density fiberboard products. *For. Prod. J.* **1999**, *49* (1), 49−56.

(9) Nazaroff, W. W.; Weschler, C. J. Cleaning products and air fresheners: exposure to primary and secondary air pollutants. *Atmos. Environ.* **2004**, *38* (18), 2841−2865, DOI: 10.1016/j.atmosenv.2004.02.040.

(10) Singer, B. C.; Destaillats, H.; Hodgson, A. T.; Nazaroff, W. W. Cleaning products and air fresheners: emissions and resulting concentrations of glycol ethers and terpenoids. *Indoor Air* **2006**, *16* (3), 179−91, DOI: 10.1111/j.1600-0668.2005.00414.x.

(11) Brown, S. K.; Sim, M. R.; Abramson, M. J.; Gray, C. N. Concentrations of volatile organic compounds in indoor air—A review. *Indoor Air* **1994**, *4* (2), 123−134, DOI: 10.1111/j.1600-0668.1994.t01-2-00007.x.

(12) Weschler, C. J.; Shields, H. C. Production of hydroxyl radical in indoor air. *Environ. Sci. Technol.* **1996**, *30*, 3250−3258, DOI: 10.1021/es960032f.

(13) Kroll, J. H.; Seinfeld, J. H. Chemistry of secondary organic aerosol: Formation and evolution of low-volatility organics in the atmosphere. *Atmos. Environ.* **2008**, *42* (16), 3593−3624, DOI: 10.1016/j.atmosenv.2008.01.003.

(14) Weschler, C. J.; Shields, H. C. Indoor ozone/terpene reactions as a source of indoor particles. *Atmos. Environ.* **1999**, *33*, 2301−2312, DOI: 10.1016/S1352-2310(99)00083-7.

(15) Weschler, C. J.; Shields, H. C. Experiments probing the influence of air exchange rates on secondary organic aerosols derived from indoor chemistry. *Atmos. Environ.* **2003**, *37* (39−40), 5621−5631, DOI: 10.1016/j.atmosenv.2003.05.007.

(16) Long, C. M.; Suh, H. H.; Koutrakis, P. Characterization of indoor particle sources using continuous mass and size monitors. *J. Air Waste Manage.* **2000**, *50*, 1236−1250, DOI: 10.1080/10473289.2000.10464154.

(17) Wainman, T.; Zhang, J. F.; Weschler, C. J.; Lioy, P. J. Ozone and limonene in indoor air: A source of submicron particle exposure. *Environ. Health Perspect.* **2000**, *108*, 1139−1145, DOI: 10.1289/ehp.001081139.

(18) Rohr, A. C.; Weschler, C. J.; Koutrakis, P.; Spengler, J. D. Generation and quantification of ultrafine particles through terpene/ozone reaction in a chamber setting. *Aerosol Sci. Technol.* **2003**, *37*, 65−78, DOI: 10.1080/02786820300892.

(19) Sarwar, G.; Corsi, R.; Allen, D.; Weschler, C. The significance of secondary organic aerosol formation and growth in buildings: experimental and computational evidence. *Atmos. Environ.* **2003**, *37* (9−10), 1365−1381, DOI: 10.1016/s1352-2310(02)01013-0.

(20) Sarwar, G.; Olson, D. A.; Corsi, R. L.; Weschler, C. J. Indoor fine particles: The role of terpene emissions from consumer products. *J. Air Waste Manage.* **2004**, *54*, 367−377.

(21) Destaillats, H.; Lunden, M. M.; Singer, B. C.; Coleman, B. K.; Hodgson, A. T.; Weschler, C. J.; Nazaroff, W. W. Indoor secondary pollutants from household product emissions in the presence of ozone: A bench-scale chamber study. *Environ. Sci. Technol.* **2006**, *40* (14), 4421−4428, DOI: 10.1021/es052198z.

(22) Singer, B. C.; Coleman, B. K.; Destaillats, H.; Hodgson, A. T.; Lunden, M. M.; Weschler, C. J.; Nazaroff, W. W. Indoor secondary pollutants from cleaning product and air freshener use in the presence of ozone. *Atmos. Environ.* **2006**, *40* (35), 6696−6710, DOI: 10.1016/j.atmosenv.2006.06.005.

(23) Vartiainen, E.; Kulmala, M.; Ruuskanen, T. M.; Taipale, R.; Rinne, J.; Vehkamäki, H. Formation and growth of indoor air aerosol

particles as a result of D-limonene oxidation. *Atmos. Environ.* **2006**, *40* (40), 7882−7892, DOI: 10.1016/j.atmosenv.2006.07.022.
(24) Alshawa, A.; Russell, A. R.; Nizkorodov, S. A. Kinetic analysis of competition between aerosol particle removal and generation by ionization air purifiers. *Environ. Sci. Technol.* **2007**, *41* (7), 2498−2504, DOI: 10.1021/es061760y.
(25) Sarwar, G.; Corsi, R. The effects of ozone/limonene reactions on indoor secondary organic aerosols. *Atmos. Environ.* **2007**, *41* (5), 959−973, DOI: 10.1016/j.atmosenv.2006.09.032.
(26) Zuraimi, M. S.; Weschler, C. J.; Tham, K. W.; Fadeyi, M. O. The impact of building recirculation rates on secondary organic aerosols generated by indoor chemistry. *Atmos. Environ.* **2007**, *41* (25), 5213−5223, DOI: 10.1016/j.atmosenv.2006.05.087.
(27) Coleman, B. K.; Lunden, M. M.; Destaillats, H.; Nazaroff, W. W. Secondary organic aerosol from ozone-initiated reactions with terpene-rich household products. *Atmos. Environ.* **2008**, *42* (35), 8234−8245, DOI: 10.1016/j.atmosenv.2008.07.031.
(28) Langer, S.; Moldanová, J.; Arrhenius, K.; Ljungström, E.; Ekberg, L. Ultrafine particles produced by ozone/limonene reactions in indoor air under low/closed ventilation conditions. *Atmos. Environ.* **2008**, *42* (18), 4149−4159, DOI: 10.1016/j.atmosenv.2008.01.034.
(29) Chen, X.; Hopke, P. K. Secondary organic aerosol from alpha-pinene ozonolysis in dynamic chamber system. *Indoor Air* **2009**, *19* (4), 335−45, DOI: 10.1111/j.1600-0668.2009.00596.x.
(30) Chen, X.; Hopke, P. K. A chamber study of secondary organic aerosol formation by linalool ozonolysis. *Atmos. Environ.* **2009**, *43* (25), 3935−3940, DOI: 10.1016/j.atmosenv.2009.04.033.
(31) Fadeyi, M. O.; Weschler, C. J.; Tham, K. W. The impact of recirculation, ventilation and filters on secondary organic aerosols generated by indoor chemistry. *Atmos. Environ.* **2009**, *43* (22−23), 3538−3547, DOI: 10.1016/j.atmosenv.2009.04.017.
(32) Chen, X.; Hopke, P. K. A chamber study of secondary organic aerosol formation by limonene ozonolysis. *Indoor Air* **2010**, *20* (4), 320−8, DOI: 10.1111/j.1600-0668.2010.00656.x.
(33) Chen, X.; Hopke, P. K.; Carter, W. P. L. Secondary organic aerosol from ozonolysis of biogenic volatile organic compounds: Chamber studies of particle and reactive oxygen species formation. *Environ. Sci. Technol.* **2011**, *45* (1), 276−282, DOI: 10.1021/es102166c.
(34) Waring, M. S.; Wells, J. R.; Siegel, J. A. Secondary organic aerosol formation from ozone reactions with single terpenoids and terpenoid mixtures. *Atmos. Environ.* **2011**, *45* (25), 4235−4242, DOI: 10.1016/j.atmosenv.2011.05.001.
(35) Liu, Q.-T.; Chen, R.; McCarry, B. E.; Diamond, M. L.; Bahavar, B. Characterization of polar organic compounds in the organic film on indoor and outdoor glass windows. *Environ. Sci. Technol.* **2003**, *37* (11), 2340−2349, DOI: 10.1021/es020848i.
(36) Weschler, C. J.; Nazaroff, W. W. Semivolatile organic compounds in indoor environments. *Atmos. Environ.* **2008**, *42* (40), 9018−9040, DOI: 10.1016/j.atmosenv.2008.09.052.
(37) Won, D.; Corsi, R. L.; Rynes, M. Sorptive interactions between VOCs and indoor materials. *Indoor Air* **2001**, *11*, 246−256, DOI: 10.1034/j.1600-0668.2001.110406.x.
(38) Singer, B. C.; Revzan, K. L.; Hotchi, T.; Hodgson, A. T.; Brown, N. J. Sorption of organic gases in a furnished room. *Atmos. Environ.* **2004**, *38* (16), 2483−2494, DOI: 10.1016/j.atmosenv.2004.02.003.
(39) Fick, J.; Pommer, L.; Åstrand, A.; Östin, R.; Nilsson, C.; Andersson, B. Ozonolysis of monoterpenes in mechanical ventilation systems. *Atmos. Environ.* **2005**, *39* (34), 6315−6325, DOI: 10.1016/j.atmosenv.2005.07.013.
(40) Flemmer, M. M.; Ham, J. E.; Wells, J. R. Field and laboratory emission cell automation and control system for investigating surface chemistry reactions. *Rev. Sci. Instrum.* **2007**, *78* (1), 014101 DOI: 10.1063/1.2432243.
(41) Springs, M.; Wells, J. R.; Morrison, G. C. Reaction rates of ozone and terpenes adsorbed to model indoor surfaces. *Indoor Air* **2011**, *21* (4), 319−27, DOI: 10.1111/j.1600-0668.2010.00707.x.
(42) Shu, S.; Morrison, G. C. Surface reaction rate and probability of ozone and alpha-terpineol on glass, polyvinyl chloride, and latex paint surfaces. *Environ. Sci. Technol.* **2011**, *45* (10), 4285−92, DOI: 10.1021/es200194e.
(43) Cano-Ruiz, J. A.; Kong, D.; Balas, R. B.; Nazaroff, W. W. Removal of reactive gases at indoor surfaces: Combining mass transport and surface kinetics. *Atmos. Environ.* **1993**, *27A* (13), 2039−2050.
(44) Weisel, C. P.; Zhang, J.; Turpin, B. J.; Morandi, M. T.; Colome, S.; Stock, T. H.; Spektor, D. M., *Relationships of Indoor, Outdoor, and Personal Air (RIOPA) Part I. Collection Methods and Descriptive Analyses*; Health Effects Institute: Boston, MA, 2005.
(45) Zhang, J.; Hartz, K. E. H.; Pandis, S. N.; Donahue, N. M. Secondary organic aerosol formation from limonene ozonolysis: Homogeneous and heterogeneous influences as a function of NOx. *J. Phys. Chem. A* **2006**, *110*, 11053−11063, DOI: 10.1021/jp062836f.
(46) Morrison, G. C.; Nazaroff, W. W. The rate of ozone uptake on carpet: Mathematical modeling. *Atmos. Environ.* **2002**, *36*, 1749−1756, DOI: 10.1016/S1352-2310(02)00156-5.
(47) Coleman, B. K. *Exposure-Relevant Ozone Chemistry in Occupied Spaces*; Department of Civil and Environmental Engineering, University of California, Berkeley: Berkeley, CA, 2009.
(48) Youssefi, S.; Waring, M. S. Predicting secondary organic aerosol formation from terpenoid ozonolysis with varying yields in indoor environments. *Indoor Air* **2012**, *22* (5), 415−26, DOI: 10.1111/j.1600-0668.2012.00776.x.
(49) Odum, J. R.; Hoffmann, T.; Bowman, F.; Collins, D.; Flagan, R. C.; Seinfeld, J. H. Gas/particle partitioning and secondary organic aerosol yields. *Environ. Sci. Technol.* **1996**, *30* (8), 2580−2585, DOI: 10.1021/es950943+.
(50) Lai, A. C. K.; Nazaroff, W. W. Modeling indoor particle deposition from turbulent flow onto smooth surfaces. *J. Aerosol Sci.* **2000**, *31* (4), 463−476, DOI: 10.1016/S0021-8502(99)00536-4.
(51) Atkinson, R.; Hasegawa, D.; Aschmann, S. M. Rate constants for the gas-phase reactions of O3 with a series of monoterpenes and related compounds at 296 ± 2 K. *Int. J. Chem. Kinet.* **1990**, *22*, 871−887.
(52) Bonn, B.; Schuster, G.; Moortgat, G. K. Influence of water vapor on the process of new particle formation during monoterpene ozonolysis. *J. Phys. Chem. A* **2002**, *106* (12), 2869−2881, DOI: 10.1021/jp012713p.
(53) Wang, H.; Morrison, G. C. Ozone-initiated secondary emission rates of aldehydes from indoor surfaces in four homes. *Environ. Sci. Technol.* **2006**, *40*, 5263−5268, DOI: 10.1021/es060080s.
(54) Morrison, G. C.; Nazaroff, W. W. The rate of ozone uptake on carpets: Experimental studies. *Environ. Sci. Technol.* **2000**, *34* (23), 4963−4968, DOI: 10.1021/es001361h.